Attitude determination model input parameters constraints for the restitution of tumbling motion of defunct satellites from photometric data

Henri Tarrieu
Aldoria, 14 rue Crespin du Gast, 75011 Paris, France
Léa Duthil, Sacha Redel, Alexis Petit
Aldoria, 14 rue Crespin du Gast, 75011 Paris, France

August 30 2024

ABSTRACT

The current orbital congestion of Low Earth Orbit (LEO) region and the Geostationnary belt has become an increasingly worrying topic amongst all stakeholders of the space community, as we have seen the number of satellite launches skyrocket in the past decade. Although some of the lower altitude debris may decay in the Earth's atmosphere on their own in short timespans, other objects like rocket bodies or defunct satellites pose a long-term threat to the health of active spacecraft and the environment. In this context, passive monitoring is not sufficient to ensure orbital safety. Some of the most promising solutions to this issue include Active Debris Removal (ADR), which is a challenging task as it requires a precise assessment of the uncontrolled target's attitude behaviour during mission design.

Attitude assessment of such uncooperative objects can be performed using photometric data from optical ground sensors, as variations of the magnitudes of Resident Space Objects (RSO) can be observed during the visible passes. The technological advances regarding ground sensors for Space Situational Awareness (SSA) purposes, both on hardware and software levels, have increased the quality, quantity and availability of photometric data of RSO. This jump in measurement acquisition capacities allows us to develop and qualify a precise light reflection model for space objects. Our proposed method is based on a three-dimensional model of the target, enabling us to simulate the object's photometric signature for any given tumbling motion and time. When optimized against photometric measurements, this model can help us perform light curve inversion, in order to extract the most likely tumbling rate and rotation axis state of the uncontrolled target. One of the major stakes of light curve inversion is the ability to reduce the parameter space of the problem, thus simplifying the photometric model based on the object physical characteristics. Without such work, the number and inter-correlatedness of variables makes the restitution of the most probable attitude solution a complex endeavor, often resulting in high uncertainty on the result. Combined with an unstable data quality due to varying environmental factors, it becomes necessary, at the very least, to know the influence of the different input parameters upon the restitution of the tumbling motion.

This paper proposes to investigate the impact of a few parameters on the attitude restitution, delving into the limitations of light curve analysis using such methods. We will thus focus on the sensitivity of our photometric model to variations of the tumbling motion itself and different object shapes. Starting with an assessment of the multi-modality of the problem caused by geometric properties, we will evaluate the efficiency of our light curve inversion algorithm through various case studies. The validity of the simulations presented for the case studies will be verified against real photometric data, ensuring the model is accurate. Considering and contrasting the results of this study, the paper concludes with potential reductions of the inversion problem, along with a presentation of the limitations of this attitude determination method and an opening on potential optimisation improvements.

Space Situational Awareness, Active Debris Removal, Photometry, Satellite Attitude Restitution, Optical Ground Sensors, Light Curve Inversion, Space Object Characterization

1. INTRODUCTION

Maintaining a comprehensive Resident Space Object (RSO) catalog has been a major stake in the development of space activities since they began. Usually, we understand "cataloguing" space objects as precisely knowing where a

given RSO is at a given time, while being able to propagate this state enough so that we can keep tracking it. This is especially important in the case of space debris, as they are very likely to cause collisions or even fragment into a multitude of smaller yet still dangerous debris in a congested orbital space.
With new space technologies focusing more and more on the mitigation and removal of the many rocket bodies (R/B) and inactive payloads still in space, arise new challenges on the characterisation of those debris. Although most "big" debris ($\geq$ 10 cm) are fairly well tracked by global Space Surveillance Awareness (SSA) ground sensor networks (optical or radar), their attitude is often poorly characterised or often unknown. This is a problem when a very comprehensive RSO catalog is needed by operators to naviguate congested spaces, even more so in Low Earth Orbit (LEO) where precise orbit determination requires precise knowledge of the target's shape and attitude. On top of this, new Active Debris Removal (ADR) missions require prior knowledge of the attitude of the uncontrolled target during the design phase. This makes us think that a fully comprehensive RSO catalog should include attitude data, monitored over time as the orbit would be. To achieve efficient attitude cataloguing, we have to develop more efficient restitution models to fit to photometric data.

In this paper, we will present our tumbling motion restitution method, delving into what makes this a complex problem. Based on important papers [1, 2], the photometry model was previously investigated to assess the detection capacity of a given RSO by an innovative optical system opening the way to optical surveys in LEO [3]. In order to focus on the light curve analysis, the model was improved, substituting the Lambert phase function by a more complex reflection law taking into account the orientation of the considered object as already proposed for attitude determination [4, 5]. Now, we propose to explore how to reduce the parameter space for light curve inversion, by asssessing its multimodality. By focusing on cylinder and box shaped objects, we target R/B and defunct satellites to understand how their physical properties influence the quality of attitude restitution. Starting with simulated case studies, we will attempt to confirm our findings by studying real photometric acquisitions of a R/B. This work will hopefully allow us to simplify or reduce the light curve inversion problem in order to obtain better restitution performances, contributing to a better maintenance of our RSO catalog.

2. MODELS

2.1 Reflective model

The photometric model for space object reflective flux estimation uses the Blinn-Phong reflection to account for all surfaces of the space object, given by [6]. This allows the simulation of diffuse and specular reflection, that are repectively independent and depend on the surface orientation relative to the observer, which is crucial in this model given the abundance of metal materials in space.

The total amount of light reflected by a surface i and received by an observer is:

$$\rho_{\text{total}}(i) = \rho_{\text{spec}}(i) + \rho_{\text{diff}}(i) \tag{1}$$

Specular reflection is given, under the flat surface assumption [6], by Eq. 2:

$$\rho_{\text{spec}}(i) = \frac{\sqrt{(n_u+1)(n_v+1)}}{8\pi} \frac{\left(u_n^I(i)\cdot u_h^I\right)^{n_u\left(u_h^I\cdot u_u^I(i)\right)^2+n_v\left(1-\left(u_h^I\cdot u_v^I(i)\right)^2\right)}}{u_n^I(i)\cdot u_{\text{sun}}^I + u_n^I(i)\cdot u_{obs}^I - \left(u_n^I(i)\cdot u_{sun}^I\right)\left(u_n^I(i)\cdot u_{obs}^I\right)} F_{\text{reflect}}(i) \tag{2}$$

where n_u along with n_v represent the smoothness of the material, $u_n^I(i)$ is the normal vector to the surface i and u_h^I is the half vector between u_{obs}^I, the observer vector, and u_{sun}^I, the incident solar vector,

$$F_{\text{reflect}}(i) = R_{\text{spec}}(i) + \left(1 - R_{\text{spec}}(i)\right)\left(1 - \mathbf{u}_{\text{sun}}^I \cdot \mathbf{u}_h^I(i)\right)^5 \tag{3}$$

is the Fresnel fraction, with $R_{spec} = R_s$ being the specular reflection coefficient of the surface.

The diffuse reflection is:

$$\rho_d(\mathbf{k}_1,\mathbf{k}_2) = \frac{28R_d}{23\pi}(1-R_s)\left(1-\left(1-\frac{(\mathbf{n}\cdot\mathbf{k}_1)}{2}\right)^5\right)\left(1-\left(1-\frac{(\mathbf{n}\cdot\mathbf{k}_2)}{2}\right)^5\right) \tag{4}$$

where R_d is the diffuse reflection coefficient of the surface, $k_1 = u^I_{obs}$ and $k_2 = u^I_{sun}$.

With respect to the energy conservation laws and for the light curve inversion that will follow, it is necessary to set conditions on the parameters, summarized in Table 1.

Table 1: Parameter conditions.

Conditions
$0 < R_d < 1$
$0 < R_s < 1$
$R_d + R_s < 1$
$n_u = n_v$
$0 < n_{u/v} < 1000$

2.2 Attitude model

Attitude determination can both be useful in the Geocentric Celestial Reference Frame (GCRF) and the body frame. Space operators mostly have access to attitude data in GCRF, but for ADR missions, knowing the attitude expressed in the body frame is crucial for docking phases. All objects are considered to be rotating in the GCRF, even at a small rate for the case of nominal attitude in controlled satellites.

The attitude model for tumbling objects requires knowledge of the initial orientation $\vec{q_0}$ that can be understood as the pointing position at t_0 and the rotation axis $\vec{q}(t)$. As a consequence, attitude determination of tumbling satellites requires fitting the initial orientation vector in GCRF as well as the rotation vector in the body frame.

In this case, from [7], the rotation states can be expressed as:

$$q(t) = \vec{q}(t-t_0)\cdot\vec{q_0} \tag{5}$$

Although this notation implies the use of quaternions, the attitude state of a satellite is expressed as rotation vectors that are converted to quaternions $\vec{\dot{\theta}}_{BF}$ for the tumbling rate and $\theta_{0,\vec{GCRF}}$ for the initial orientation, where:

$$\vec{\dot{\theta}}_{BF} = \dot{\theta}_{x,BF}\cdot\vec{x_{BF}} + \dot{\theta}_{y,BF}\cdot\vec{y_{BF}} + \dot{\theta}_{z,BF}\cdot\vec{z_{BF}} \tag{6}$$

$$\theta_{0,\vec{GCRF}} = \theta_{x,GCRF}\cdot\vec{x_{GCRF}} + \theta_{y,GCRF}\cdot\vec{y_{GCRF}} + \theta_{z,GCRF}\cdot\vec{z_{GCRF}} \tag{7}$$

Thus the problem contains a minimum of 6 degrees of freedom.

3. MULTI-MODALITY ASSESMENT

The high number of parameters in our model justifies the use of a Markov Chain Monte Carlo (MCMC) [8] algorithm to fit photometric data. Thus, it is important to assess the multimodality of the problem, as classical proposals in the parameter space showed poor performance. This is notably necessary in the case of tumbling objects, since few assumptions can be made on their attitude. As such, we focus on the attitude parameters, since the reflective coefficients can be given by the satellite manufacturer or estimated from statistical sources [9].

Since the rotation axis is expressed in the body frame and the initial orientation is in GCRF coordinates, one can notice that applying a rotation α on the tumbling axis of the satellite in a given plane and applying an equal counter-rotation $-\alpha$ on the initial orientation along the same revolution axis yields the same rotation vector in the GCRF, which could consequentially lead to the same photometric signature. We can do so by using various orientations of the rotation

vector, offset by an angular distance β to the considered plane. This should allow us to show the intricacies and correlations between the rotation vector $\vec{q}(t)$ and the initial orientation $\vec{q}_0$. Fig. 1 shows this method.

Using this process, one can qualitatively assess the multimodality of the problem.

With the notation used in Eq. 7 to describe the initial orientation vector $\vec{q}_0$ components while ensuring that $\|\vec{q}_0\| < \pi$, we can initially define their existence intervals as:

$$\theta_{x,GCRF} \in]-\pi,\pi],\ \theta_{y,GCRF} \in]-\pi,\pi],\ \theta_{z,GCRF} \in]-\pi,\pi], \tag{8}$$

Studying the influence of the rotation along each axis of the space object will allow us to demonstrate the impact of symmetries on the multimodality of the problem.

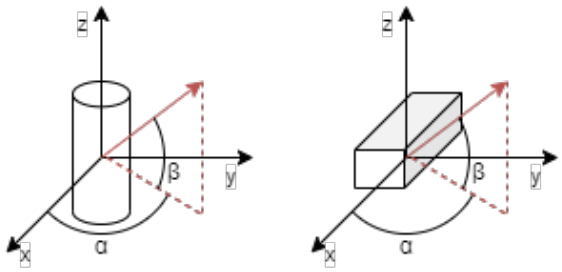

Fig. 1: 3D representation on the angles and vectors used to determine the modes due to symmetries in the objects geometry. By countering the rotation α of the rotation vector along the Z-axis with a rotation $-\alpha$ of the initial orientation, the resulting rotation vector in GCRF coordinates will remain unchanged.

First, the cylindrical shape will be evaluated, corresponding to a Rocket Body (R/B), since this shape is widely common in Earth Orbit. This will be followed by the evaluation of a box shaped satellite, with no solar arrays or specific features. Finally, we will estimate the impact of the modelisation of such features on the multimodality of the problem.

For each shape, the 3 planes of symmetry will be evaluated. Since the objective at hand still consists in fitting the attitude of a satellite to a photometric data series, we will compute the Mean Square Error (MSE, given in Eq. 9) of each fitted curve compared to a well defined simulated one, which remains the same throughout the study, whose attitude parameters are given in Table 2:

Table 2: Attitude parameters of the synthetic light curves.

Parameter	Value	Unit
$\|\dot{\theta}\|$	0.026	rad/s
β	0	rad
α	0	rad

$$MSE = \sum_{i=1}^{D} (x_i - y_i)^2 \tag{9}$$

Where x_i is a magnitude value on the reference light curve, y_i is a point on the evaluated light curve and D is the number of points on the light curve.

One can note that two different light curves might have the same MSE relative to the reference one, while being different to one another. However the goal of this evaluation is to assess the limits of light curve fitting, so the use of a simplified cost function to extract the different modes is relevant in this case.

3.1 Cylinder

In this section, we start by studying the effect of symmetries on this problem for a cylindrical shaped object. Physical properties of the object are given in Table 3. All surfaces possess the same reflective properties. In Fig. 2, we

demonstrate that the solution space shows continuous areas that minimize MSE, which would yield the same light curve as the one simulated in this exercise, despite the fact that corresponding rotation vectors are different from the simulated one.

Table 3: Physical properties of the cylinder shape object.

Parameter	Value	Unit
Diameter	4.2	m
Length	21	m
R_d	0.8	-
R_s	0.01	-
$n_{u,v}$	10	-

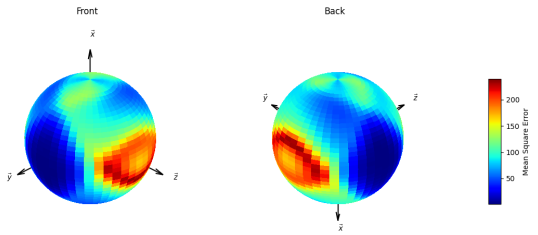

Fig. 2: 3D representation of the Mean Square Error (MSE) for all initial rotations along $\vec{x_{BF}}$ for a cylinder with a Length to Diameter (L/D) ratio of 5.

The cylindrical shape presents many symmetries, the most notable being the revolution symmetry. This can be seen on Fig. 3, where a fixed orientation β of the rotation vector yields the same MSE for all α orientations in the XY plane.

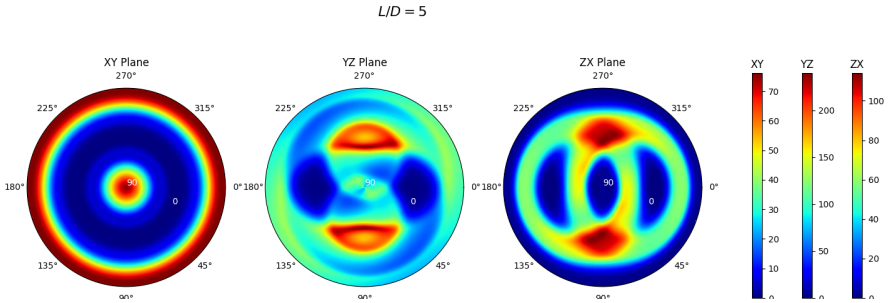

Fig. 3: Identification of the modes for the rotation in each plane of the body frame for a cylindrical shape with $L/D = 5$ from the MSE measurements using a polar projection. The impact of the circular symmetry along the Z-axis is clearly visible on the XY plane figure.

Therefore, evaluating the z component $\theta_{z,GCRF}$ of the initial orientation of the body frame in GCRF might not be relevant and adds many modes to the problem. It is thus possible to discard this component in the case of a cylinder. Regarding the rotation along the x and y axes of the body frame, one can note an axial symmetry, as it is possible to "fold" the polar representations once. Hence, it could be possible to limit the parameter space of $\theta_{x,GCRF}$ and $\theta_{y,GCRF}$ by fitting on only half the possible values. The choice of the bounding values is quite important, as it is necessary to limit the number of discrete attraction points, represented by the areas yielding low MSE. However, in this case, we choose not to restrain the boundaries of the parameters, and to only focus on the dimension reduction of the problem by discarding solutions along the z axis, as shown in Table 3.1.

Table 4: $\vec{q}_0$ components bounds for cylindrical configuration.

Parameter	Lower bound	Upper bound	Unit
$\theta_{x,GCRF}$	$-\pi$	π	rad
$\theta_{y,GCRF}$	$-\pi$	π	rad
$\theta_{z,GCRF}$	-	-	rad

3.2 Box

From the study of the cylinder case, it is possible to deduce that only revolution symmetries can reduce the number of initial orientation vector $\vec{q}_0$ components required to fit light curves in a valid parameter space. Let us see the case of a box satellite to assess the veracity of such a claim, shown on Fig. 4.

The object's physical properties are given in Table 5. All surfaces present the same reflective properties.

Table 5: Physical properties of the box shaped object.

Parameter	Value	Unit
Length	5	m
Height	2.5	m
Depth	3.75	m
R_d	0.4	-
R_s	0.1	-
$n_{u,v}$	10	-

It is clear that planar symmetry cannot reduce the number of fitting parameters. However, one can note that it is possible to bound them along each plane of symmetry. This is even clearer in the case of a cube, shown on Fig. 5.

The small differences in MSE values that break symmetry are due to the reference frame change applied to the rotation vector to be expressed in the GCRF, leading to small discrepancies propagated and emphasized with time. This is less visible for the cylinder case as the curved surfaces it contains tend to smoothen out these features, and little specular reflection is produced since $R_s = 0.01$ for cylinders and $R_s = 0.1$ for boxes.

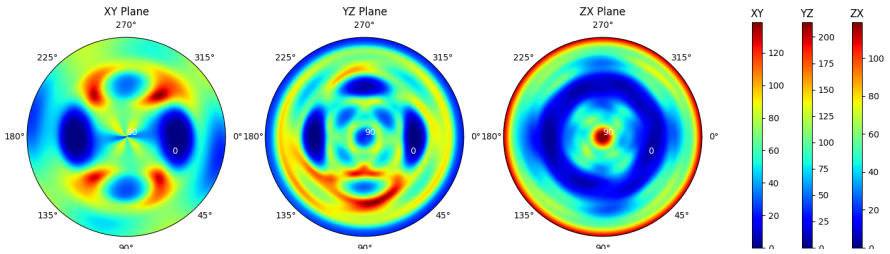

Fig. 4: Identification of the modes for the rotation along each plane of the body frame of the box shape from the MSE residuals. Modes can be found on all planes, although not completely symmetrical, mostly due to the reference frame change applied to the rotation vector to be expressed in the GCRF and the specular reflection used for this object.

Therefore, it seems like the number of dimensions of the initial orientation vector for a box shaped satellite cannot be reduced. Moreover, some discrete ranges of (α, β) can yield the same MSE, though they are not linked. This could potentially be a problem while fitting the values as the parameters could stay stuck in one region during MSE minimization.

3.3 Impact of the addition of features

To conclude on the effect of geometry on the modes of the problem, it is interesting to evaluate a satellite presenting features, as solar arrays or other elements can be present. We propose to add one solar array on one side and to evaluate the resulting modes, given in Fig. 6. The solar arrays photometric properties are given in Table 6.

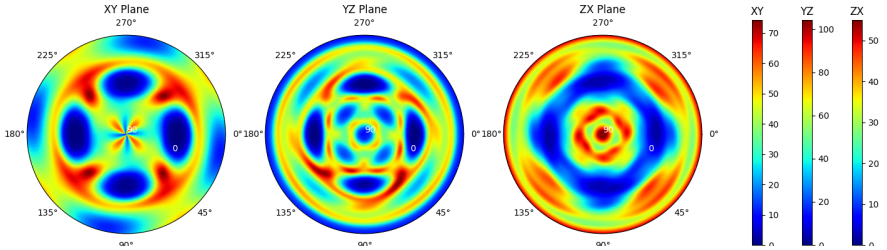

Fig. 5: Identification of the modes for the rotation along each plane of the body frame of the cube shape from the MSE residuals. The impact of the planar symmmetry is clearly visible for all planes.

Table 6: Physical properties of the solar array.

Parameter	Value	Unit
Length	5	m
Height	2.5	m
R_d	0.01	-
R_s	0.6	-
$n_{u,v}$	100	-

Since the solar array is offset from the geometrical center and on the XY axis, we can see no apparent difference in the modes when rotating the satellite along $\vec{z}$. However, the symmetry is broken on the other axes, with an increase of the MSE gradient due to the high specularity of the solar array. This leads to a wider range of possible initial orientatiosn to render the full parameter space.

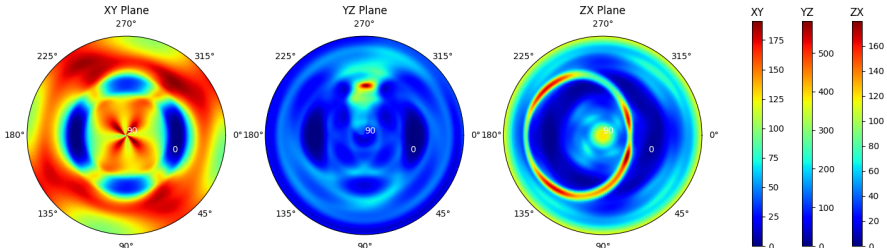

Fig. 6: Identification of the modes for the rotation in each plane of the body frame of the cube shape from the MSE residuals. The impact of the planar symmmetry is clearly visible for all planes.

Keeping in mind that box shaped objects are rarely homogenous by their materials and usually present features, it is advisable to maintain the default bounds for such objects, shown in Table 7.

Table 7: $\vec{q_0}$ components bounds for box shaped objects.

Parameter	Lower bound	Upper bound	Unit
$\theta_{x,GCRF}$	$-\pi$	π	rad
$\theta_{y,GCRF}$	$-\pi$	π	rad
$\theta_{z,GCRF}$	$-\pi$	π	rad

We will thus focus on the impact of component bounds and dimension reduction for cylindrical objects.

3.4 Conclusion on multimodality

It is clear that only specific conditions have been investigated to reduce the parameter space. This is quite a difficult task as the rotation rate and initial orientation vectors can vary. Evaluating all the possible configurations that yield

the same mean square error requires to assess for any given light curve the resulting modes, on all 5 or 6 attitude parameters depending on the shape of the object.

In addition, it is possible to reduce multimodality of the problem by using various reflective coefficients for each surface, which tends to a more realistic approach. However, this can require the fitting of reflective parameters, for which, in the case of tumbling objects, adds more complexity to the problem, and possibly more modes in the solution space.

For the restitution of the rotation rate from photometric data, without prior knowledge, it is possible to extract the light curve period using frequency analysis, and focus on the tumbling axis by constraining the possible values of the rotation rate vector norm to specific ranges. Given ththat some symmetries might yield a frequency that is not the real tumbling rate of the object but a harmonic, it is possible to envision choosing n times the rotation period according to the object's shape.

4. STUDY ON SIMULATED DATA

After showing the high multimodality of the attitude restitution problem, we will verify some of the hypothesis that emerged on the possible reductions of the initial parameter space. Before this, we review different methods for fitting parameters to simulated data, in order to ensure that further research is not biaised by an algorithm that struggles to explore the full parameter space.

4.1 Assessing the need for differential evolution for parameter proposals

The main objective of this section is to assess the impact of the fitting functions for various aspect ratios of cylinders L/D by evaluating the restitution of the rotation rate and the tumbling axis.

It will focus on the study of the attraction points yielded by the Monte Carlo inversion process. Since the problem is highly multimodal, let us evaluate the impact on the restitution of the metrics described above with proposals generated using Differential Evolution (DE) [10], as advised by [11], compared to classical stretch moves.

Keeping in mind that the objective at hand is to determine the tumbling axis and the rotation rate, and given that the initial orientation fitted is a consequence of the attitude model, this metric will not be evaluated here.

Fig. 7 gives the fitting results of the rotation rate. Using stretch moves gives more weight to the rotation rate harmonics, for any L/D ratio. One can note the influence of L/D on the convergence of the values: decreasing the aspect ratio yields less convergence, as the Kernel Density Estimation (KDE) possess wider Full Width at Half Maximum (FWHM), given in Table 8.

Table 8: Main density peaks of the rotation rate obtained by the fitting algorithm for stretch and DE moves.

Moves	Stretch			Differential Evolution		
L/D	$\|\dot{\theta}(\rho_{max})\|$	ρ_{max}	FWHM	$\|\dot{\theta}(\rho_{max})\|$	ρ_{max}	FWHM
1	0.052	13.400	0.007	0.026	44.095	0.003
2	0.105	8.888	0.009	0.026	25.461	0.005
5	0.053	26.782	0.003	0.026	72.488	0.002

Fig. 8 shows the impact of the aspect ratio on the fitting results of the rotation vector. For larger aspect ratios, it is possible to observe better convergence of the values, with more KDE peaks occuring for small aspect ratios. This can also be confirmed when considering Fig. 10 and 9, upon which we can see more points of attraction on the YZ plane for $L/D = 1$ compared to $L/D = 2$.

When considering the influence of stretch moves relative to DE moves, the latter yield better convergence towards the correct value, giving less importance to incorrect modes. Furthermore, convergence towards the correct value is less affected by the aspect ratio, as no global trend can be observed in the value of the density peaks given in Table 9.

Considering the results seen in this section, it is advisable to use differential evolution for parameter proposal to fit symmetrical objects, especially when dealing with high multimodality.

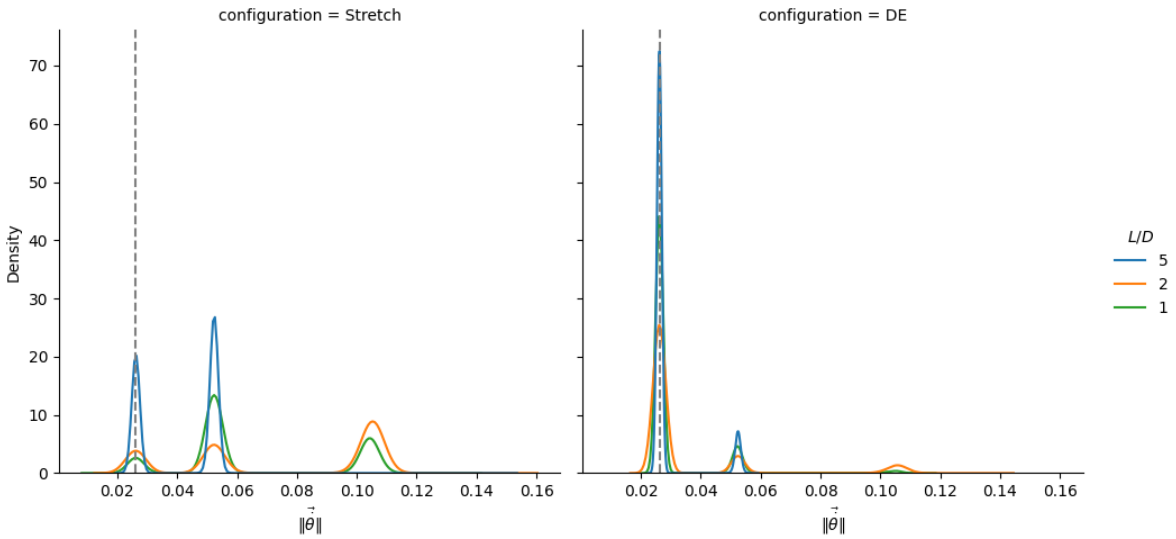

Fig. 7: Tumbling rate restitution for stretch and DE moves. In the case of the stretch move on the left hand side, the restitution of the correct tumbling rate decreases with the aspect ratio of the cylinder. When using DE, the algorithm converges better towards on the correct rotation rate displayed by the dashed line.

Table 9: Main density peaks of the tumbling vector direction obtained by the fitting algorithm for stretch and DE moves.

Moves	Stretch			Differential Evolution		
L/D	$\beta(\rho_{max})$	ρ_{max}	FWHM	$\beta(\rho_{max})$	ρ_{max}	FWHM
1	65.440	0.003	27.469	-0.030	0.027	5.468
2	-79.104	0.003	18.409	-0.038	0.019	6.745
5	-0.026	0.005	11.177	0.072	0.030	4.663

the

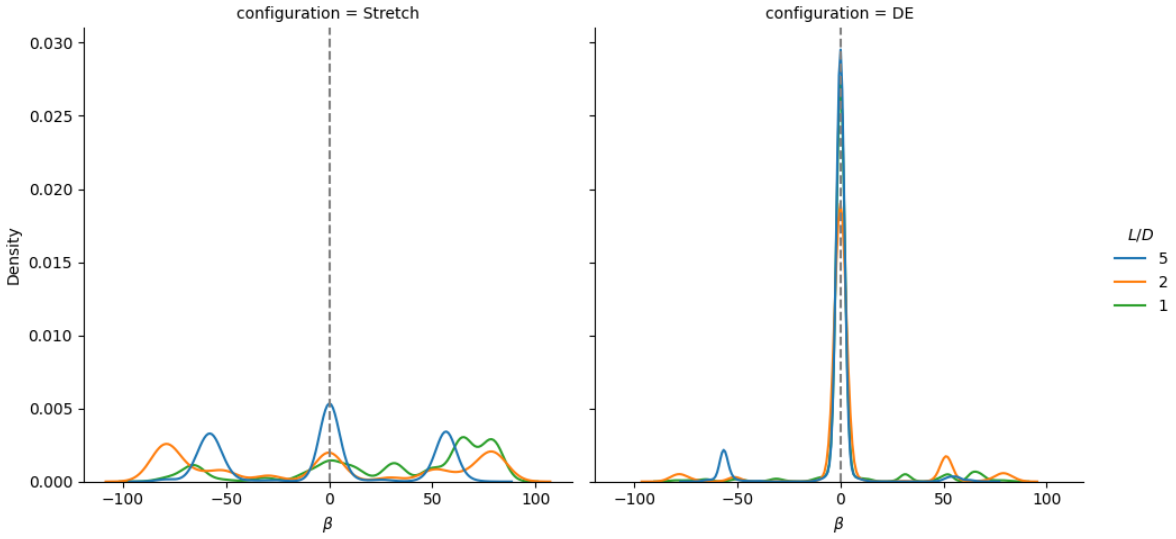

Fig. 8: Angular distance (in degrees) of the rotation vector to the XY plane restitution for stretch and DE moves. In the case of the stretch move on the left hand side, the convergence decreases with the aspect ratio, as many centers of attraction can be seen for $L/D = \{1, 2\}$. Once again, DE yields better convergence towards the correct value.

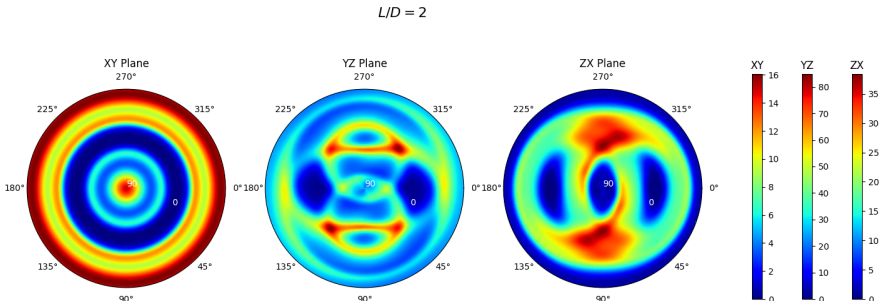

Fig. 9: Identification of the modes for the rotation in each plan of the body frame of the cylindrical shape with $L/D = 2$ from the MSE residuals using a polar projection. When comparing with $L/D = 5$, more attraction points occur in the YZ plane.

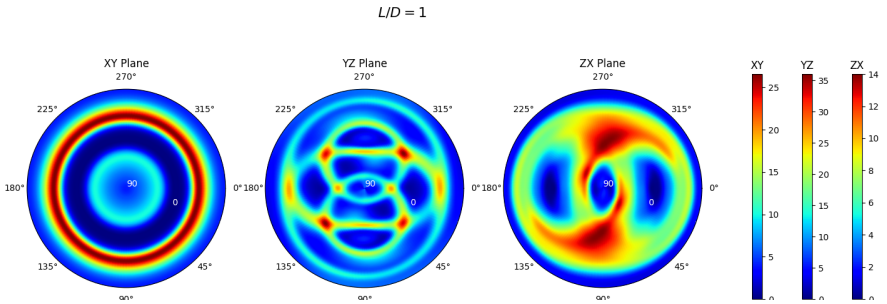

Fig. 10: Identification of the modes for the rotation in each plane of the body frame of the cylindrical shape with $L/D = 1$ from the MSE residuals using a polar projection. When comparing with $L/D = 2$, more attraction points occur in the YZ plane.

4.2 Effect of dimension reduction

Let us study the assumptions made in Section 3 regarding the fitting parameters. Using DE moves, since this proposal function allows for better performance and convergence, the influence of fitting the initial orientation $\theta_{z,GCRF}$ will be evaluated on the same dataset.

Table 10: Main density peaks of the rotation rate obtained by the fitting algorithm for default and cylinder configurations using DE moves. Constraining the initial rotation vector decreases the fitting accuracy for high L/D values.

Bounds	Default			Cylinder		
L/D	$\beta(\rho_{max})$	ρ_{max}	FWHM	$\beta(\rho_{max})$	ρ_{max}	FWHM
1	0.026	44.095	0.003	0.026	64.789	0.002
2	0.026	25.461	0.005	0.026	51.859	0.003
5	0.026	72.488	0.002	0.053	29.616	0.003

Fig. 11 shows that discarding the fitting of the $\theta_{z,GCRF}$ component of the initial orientation leads to better convergence when dealing with highly multimodal problems such as low L/D values. When considering the density peak values given in Table 10, setting $\theta_{z,GCRF} = 0$ leads to a density peak increase of 45% for $L/D = 1$ and 25% for $L/D = 2$. Yet, for high aspect ratios, two peaks appear, the densest giving twice the correct rotation rate. Thus, we can assume that, while using a 2D initial orientation vector by discarding $\theta_{z,GCRF}$ leads to increasingly better convergence towards the right rotation rate values with lower aspect ratios, it is not optimal for high L/D values.

Now looking at the tumbling axis restitution from Fig. 12, we can notice the high β value of the convergence peak for $L/D = 5$ with the cylinder configuration, yielding more rotation along the revolution axis of the body frame than the flat-spin axis. While being less noticeable for the default configuration, this peak is still present around the same absolute value of 57°. Both peaks appear due to symmetry while having different density values. Their occurence is

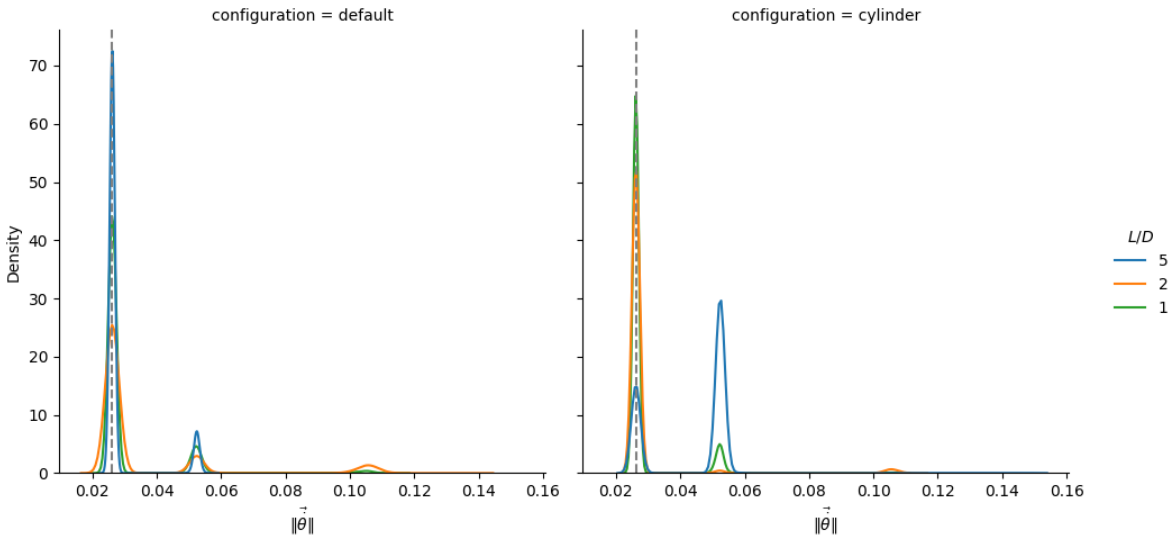

Fig. 11: Rotation rate restitution for default and cylinder configurations using DE moves. In the case of the cylinder configuration on the right hand side, the restitution of the rotation rate decreases with the aspect ratio of the cylinder. When using the default configuration, better convergence towards the correct value is achieved for high aspect ratios.

Table 11: Main density peaks of the tumbling vector direction obtained by the fitting algorithm for default and cylinder configurations using DE moves. Constraining the initial rotation vector decreases the fitting accuracy for high L/D values.

Bounds	Default			Cylinder		
L/D	$\beta(\rho_{max})$	ρ_{max}	FWHM	$\beta(\rho_{max})$	ρ_{max}	FWHM
1	-0.030	0.027	5.468	0.476	0.033	4.452
2	-0.038	0.019	6.745	-0.253	0.042	3.632
5	0.072	0.030	4.663	57.196	0.008	9.817

due to the large range of β values that yield a similar MSE value from Fig. 3 when considering the XY plane.

Thus, the restitution of the correct rotation rate and axis is highly dependent on the aspect ratio. Fitting those parameters for R/B therefore requires prior knowledge of this parameter in order to yield accurate results.

5. CYLINDER TYPE REAL OBJECT

In this section, we propose to test the assumptions deduced from work on simulated data on a real case. Studying light curves acquired by the ALDORIA network, we will also test reducing the problem in terms of acceptable rotation rate range by performing frequency analysis prior to attempting tumbling motion restitution.

5.1 Using frequency analysis for better parameter restriction

From Fig. 13, presenting the spectra for each aspect ratio of the light curves considered, it is possible to assume that any flat-spin axis rotation in the body frame will lead to a main rotation period that is twice or four times the real frequency. Consequently, we can assume that the real rotation rate will not be represented on the frequency analysis, and that bounding the tumbling rate as an input might lead to better attitude resitution. Moreover, as it can be seen for aspect ratios of 1 and 2, the more flat surfaces contribute to the light curve, the higher the secondary frequency peak will be. Thus, for small aspect ratios, taking half the rotation rate of the first peak is advisable for an initial rotation rate estimate.

From the study of the synthetic results and Fig. 14, it is possible to estimate the rotation rate of CZ-3B R/B #59707 around $0.042\,rad/s$. Since we can assume that within the observation range the object's rotation is constant, we can

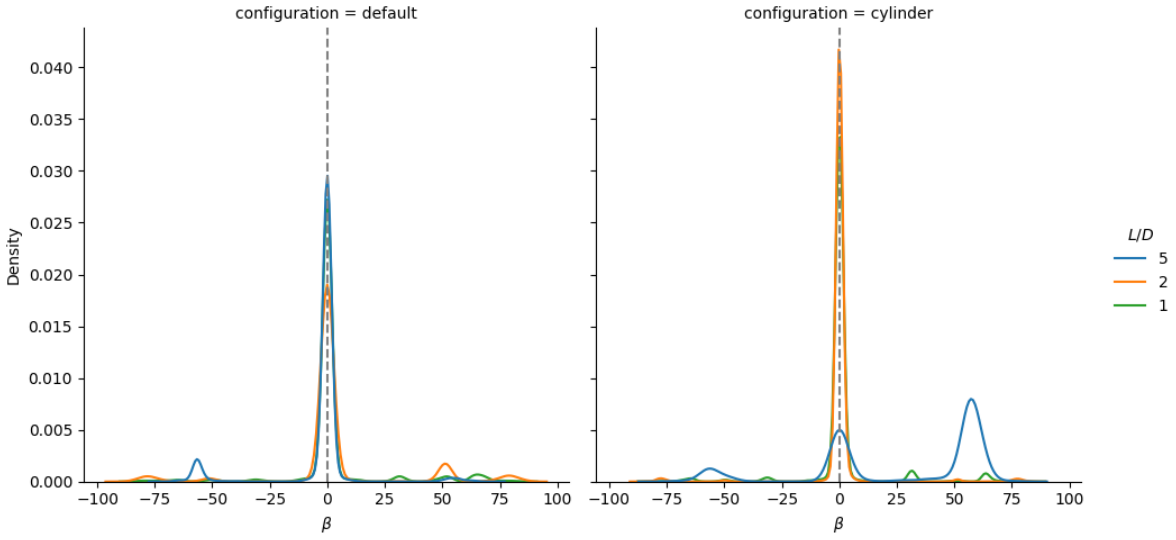

Fig. 12: Tumbling vector direction restitution for default and cylinder configurations using DE moves. In the case of the cylinder configuration on the left hand side, the restitution of the tumbling rate decreases with the aspect ratio of the cylinder. When using the default configuration, better convergence towards the correct value is achieved for high aspect ratios.

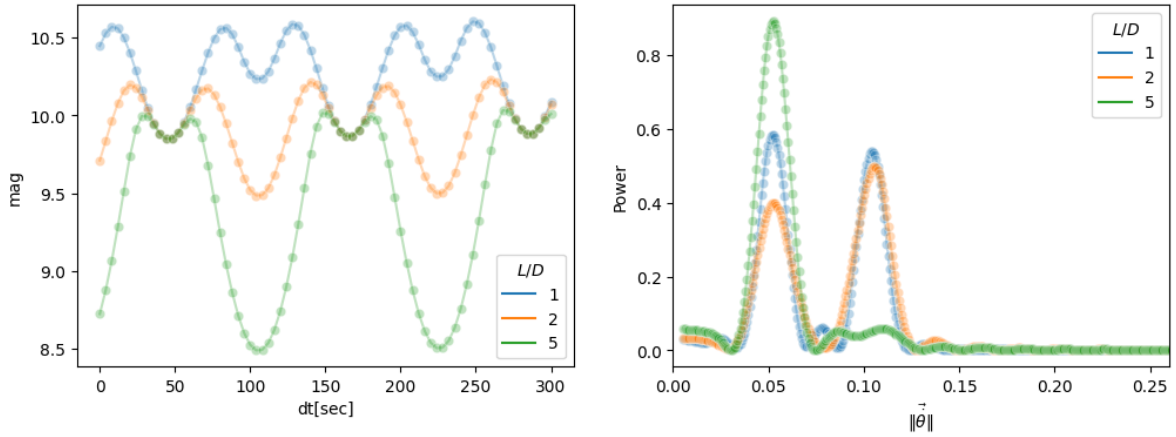

Fig. 13: Frequency analysis of the light curves generated for a same pass with different L/D ratios. While the true rotation rate is $0.026\,rad/s$, for aspect ratios of 5 and 1, the main rotation rate extracted is twice as fast. For $L/D = 2$, the main frequency is 4 times that of the real one, but the second most powerful peak has the same value as the other ones.

explain the spectrum differences with the observation conditions that yield varying significant contributions of the flat faces to the luminous flux reflected off the object, which validates the assumption made above.

While the light curve aquisition of the 2024/08/06 presents higher variations and more contributing surfaces, its solar phase angle is about 130°, which from experience is too significant to yield correct reflection in the model. Thus, the rest of the study will focus on the 2024/08/09 observation, with a phase angle of approximately 100° throughout the acquisition.

5.2 Results

Let us now evaluate the fitting on a real R/B type object, whose properties are given in Table 12.

Given the high value of the aspect ratio L/D, and its known geometry, this section will focus on the influence of the

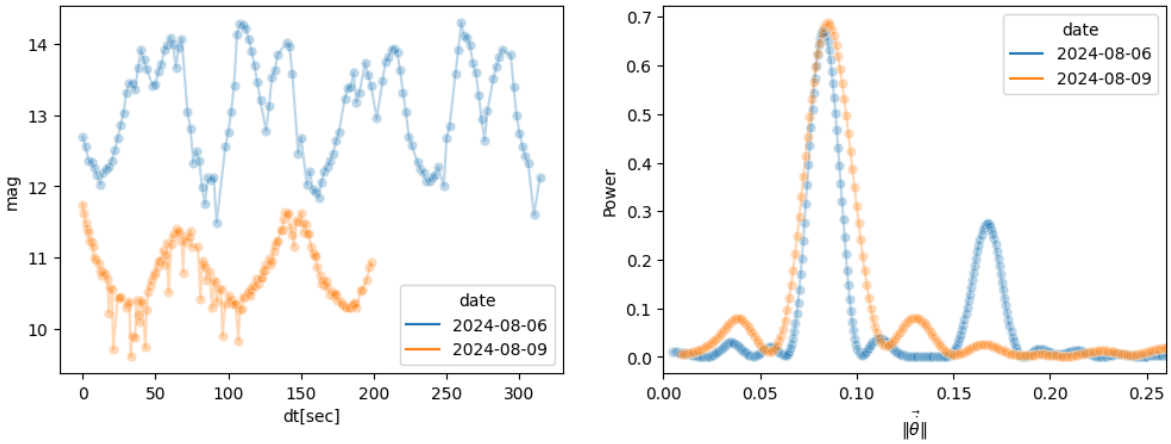

Fig. 14: Frequency analysis of the photometric signature of CZ-3B R/B #59707 at two given dates. From the magnitudes variations on the left hand figure, it is possible to deduce a tumbling motion, confirmed by the frequency analysis on which a clear frequency peak is visible on both light curves at $0.084\,rad/s$. On the data acquired on 2024/08/06, a secondary peak can be seen, due to the object's orientation leading to more light reflected off the flat faces of the cylinder.

Table 12: Properties of the R/B studied.

Property	Value	Unit
Name	CZ-3B R/B	-
NORAD ID	59707	-
Diameter	3	m
Length	12.3	m
L/D	4.1	-

relfection parameters. We will evaluate the attitude restitution for two cases:

1. The object is homogenous, where all surfaces have the same reflective properties;
2. The object is heterogenous, where the curved surface is composed of a different material than that of the flat faces of the cylinder.

Nevertheless, since fitting parameters have been added, the effect of reducing attitude parameters will also be evaluated. Hence, the unknown factor will be the diffuse and specular reflection values R_d and R_s, which we will try and fit simultaneously with the attitude. We will then compare the tumbling axis with the expected one, which according to [12] is mostly radial for R/B type space debris.

Let us refer to the terms used in the figures referenced in this section with Table 13.

Table 13: Fitting model configurations.

	Default		$\|\dot{\theta}\|$ bounded	
$n_{materials}$	$\|\dot{\theta}\|$	$\theta_{z,GCRF}$	$\|\dot{\theta}\|$	$\theta_{z,GCRF}$
1	< 0.15	$\in]-\pi,\pi]$	< 0.075	$\in]-\pi,\pi]$
2	< 0.15	$\in]-\pi,\pi]$	< 0.075	$\in]-\pi,\pi]$

Fig. 15 gives the distribution of the rotation rates evaluated throughout the fitting. When considering the default configuration, adding a second material has not led to better fitting, as the peak around the expected value of $0.042\,rad/s$ is not present for $n_{materials} = 2$. This can be explained by the little contribution of the flat surfaces of the cylinder on the

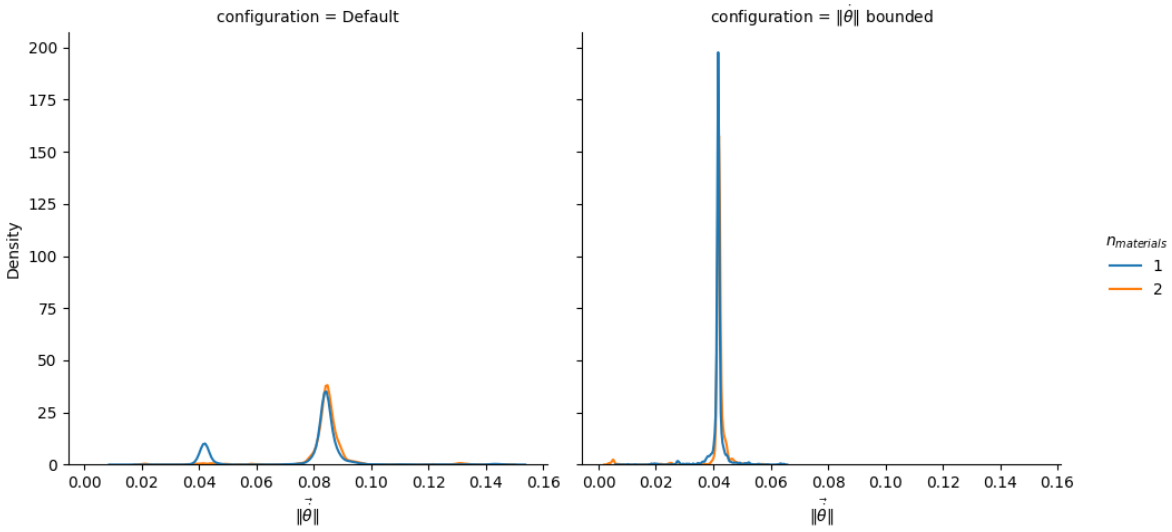

Fig. 15: Restitution of the rotation rate for CZ-3B R/B, using default and bounded rotation configuration and modeling 1 or 2 materials on the R/B. While the default configuration results are in accordance with the frequency analysis, the expected rotation rate is not the main point of convergence. By bounding the rotation vector, only one clear density peak on the expected rotation rate is found. Regarding the impact of materials modeled with this configuration, no apparent trend can be found.

measured data, that do not specifically require fitting since they do not reflect much light given the object's orientation during the pass. Bounding the rotation rate has allowed for far more convergence towards the correct estimated value, for all cases.

Let us now consider the orientation of the rotation vector within the body frame, shown on Fig. 16. With the default configuration, two clear concentration points are visible for both cylinder models. The results are highly unlikely, with a strong revolution axis component. It also seems like the maximum concentration of values with a bounded rotation rate does not yield better results. Nonetheless, a third density peak occurs for $\beta = 0^\circ$, with this configuration. Furthermore, the addition of a second material to model the R/B yields higher convergence towards that value.

To further understand the intricasies of the fitting results, let us consider Fig. 17, showing the light curves corresponding to the maximum likelihood, i.e the densest region of the fitting parameter results and the physically accurate peak giving a rotation mostly along the flat-spin axis, compared to the measured data.

The first observation is that although outliers have not been removed, they do not interfere with the fitting. Secondly, the raw data suggests that specular reflexion at $150\,s$ occurs for the flat surface, but no result has been able to reproduce this peak, whether it be the physically accurate guess or the most likely. It is possible that a specular peak also occurs at $75\,s$, but given the outliers in the data it is difficult to clearly assess this. Finally, both guesses present the same rotation rate, visible on Table 14, showing the limits of the inversion due to the problem's high multimodality. Now looking at the reflective properties obtained on this table, one can notice the high value of $R_{d,curved}$ for the most likely state compared to that of the physically accurate. This can be explained with the strong revolution axis component of the rotation vector, yielding less cross section variations during the pass combined with poor reflection due to its initial orientation, and thus requiring higher value of the diffuse reflection coefficient. Yet, the value obtained for the physically accurate guess seems quite small for a white paint coated object. When focusing on the specular reflection of the curved surfaces, where the physically accurate guess provides high $R_{s,curved}$ values, neither seem consistent with the properties of the R/B. Nevertheless, the reflective coefficients of the flat surfaces are in accordance for both guesses, showing their negligeable contribution to the photometry. This is the case for the attitude model did not give attitude guesses that make them contribute to the light curve, especially towards the magnitude peaks.

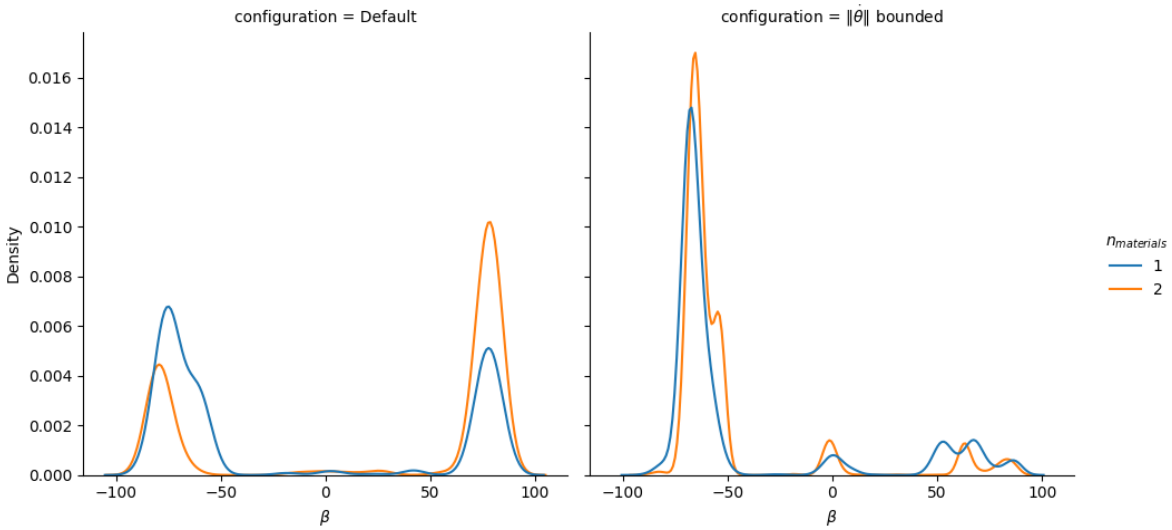

Fig. 16: Restitution of the tumbling vector orientation for CZ-3B R/B, using default and bounded rotation configuration and modeling 1 or 2 materials on the R/B. With the default configuration, we can notice that converging towards twice the expected rotation rate yields physically inaccurate tumbling vector orientations. While this remains the case with the bounded configuration, more values converge towards a physically accurate value, slightly increased when the model is closer to reality by simulating 2 materials.

Table 14: Fitting results for the inversion of CZ-3B R/B observed on the 2024/08/09 with 2 materials modeled and bounded rotation rate.

Parameter	Most likely	Physically accurate	Unit
$\|\dot{\theta}\|$	0.0421	0.0423	rad/s
β	-65	0	$^\circ$
$R_{d,curved}$	0.9	0.29	-
$R_{s,curved}$	0.04	0.62	-
$R_{d,flat}$	0.02	0.08	-
$R_{s,flat}$	0.29	0.22	-

6. CONCLUSION

Light curve inversion for tumbling objects presents high multimoality, therefore increasing the number of possible results through MCMC fitting. Nevertheless, it is possible to reduce the multimodality of the problem by discarding the fitting of some parameters, such as the initial orientation of the object.

Considering the inversion of highly symmetrical RSO such as R/B, it has been shown that, given their high multi-modality, it is possible to reach better convergence by using a different proposal function than the classical stretch move. The reduction of the fitting parameters can be quite useful for better convergence on multiple attitude parameter values, but is highly dependent on the aspect ratio L/D of cylindrical objects. The veracity of the solution still requires analysis, by evalutating the physical accuracy of the rotation vector within the body frame. There are ways to enhance the convergence of the parameters towards a physically correct value, such as:

- Using the object inertia rather than simple rotation;
- Fitting the reflective coefficients with nominally functionning objects. In the case of R/B, this would require observing the objects just after separation, since their tumbling motion usually increases over time once they become debris;
- Bounding or discarding the revolution axis component of the rotation vector;

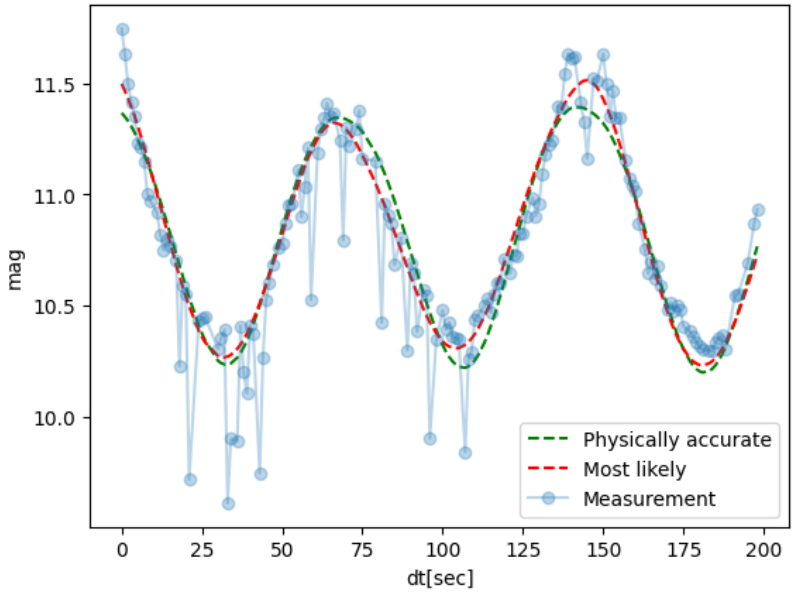

Fig. 17: Fitted light curves for both guesses considered compared to measured magnitudes during the 2024/08/09 pass for CZ-3B R/B #59707. Both guesses, while giving clearly different rotation vectors show almost identical photometric signatures, due to high multimodality for large L/D aspect ratio.

- Observing the object with a small phase angle for the reflection model to yield non zero flux values throughout the whole light curve for any set of parameters;
- Using frequency analysis to estimate the number of contributing surfaces and materials.

While the study on simulated data has shown efficient convergence towards physically accurate values compared to real observations, this is due to the small solar phase angles of the synthetic light curves generated, as the object was on a Geostationnary Orbit (GEO). For comparison, CZ-3B R/B that was observed and whose photometric measurement where the subject of the real case inversion section was on a Highly Elliptical Orbit (HEO) and had high solar phase angle values, rendering difficult the inversion given the geometrical approximations made to model the object.

From this observation, two assumptions can be made. First, light curve inversion of low altitude objects such as LEO or HEO near their perigee represents in itself a challenge, as solar phase angle values vary significantly during a pass and can attain high values. Second, the analysis of the fitting results, given the high multimodality, requires a different method than the usual approach. Indeed, it is necessary to study the physical veracity for each density point of the parameters, which in this study has been done throughout Kernel Density Estimation. Therefore, it is not specifically required to reduce the parameter bounds or to discard them, if it is desired to develop a general case algorithm.

It has also been shown that frequency analysis for symmetrical objects only gives a rotation rate harmonic, and that symmetry assessment is required to bound the rotation rate values in order to discard those harmonics that tend to yield irrelevant rotation axis values. Such prior spectral analysis has its advantages, as it allows to bound the rotation axis values.

Light curve inversion through MCMC fitting has its limits, and much can be investigated to enhance the performance of such a method, either by optimizing it or combining it with other approaches.

REFERENCES

[1] J. R. Shell, "Optimizing orbital debris monitoring with optical telescopes," in *Advanced Maui Optical and Space Surveillance Technologies Conference*, p. E42, 2010.

[2] A. Milani, D. Farnocchia, L. Dimare, A. Rossi, and F. Bernardi, "Innovative observing strategy and orbit determination for low earth orbit space debris," *Planetary and Space Science*, vol. 62, no. 1, pp. 10–22, 2012.

[3] A. Petit, R. Lucken, H. Tarrieu, D. Giolito, and T. Lépine, "Share my space multi-telescope observation stations performance assessment," 2021.

[4] R. Linares, M. K. Jah, and J. L. Crassidis, "Inactive space object shape estimation via astrometric and photometric data fusion," *Adv. Astronaut. Sci.*, vol. 143, pp. 217–232, 2012.

[5] B. K. Bradley and P. Axelrad, "Lightcurve inversion for shape estimation of geo objects from space-based sensors," in *Univ. of Colorado. International Space Symposium for Flight Dynamics*, 2014.

[6] M. Ashikhmin and P. Shirley, "An anisotropic phong light reflection model," Tech. Rep. UUCS-00-014, University of Utah, Salt Lake City, UT, 2000.

[7] A. D. Team, "Attitude from angular rate," 2024. Accessed: 2024-08-15.

[8] J. Goodman and J. Weare, "Ensemble samplers with affine invariance," *Communications in Applied Mathematics and Computational Science*, vol. 5, pp. 65–80, 2010.

[9] M. K. Mulrooney, M. J. Matney, M. D. Hejduk, and E. S. Barker, "An investigation of global albedo values," in *Advanced Maui Optical and Space Surveillance Technologies Conference*, pp. 624–633, 2008.

[10] B. Nelson, E. B. Ford, and M. J. Payne, "Run dmc: An efficient, parallel code for analyzing radial velocity observations using n-body integrations and differential evolution markov chain monte carlo," *The Astrophysical Journal Supplement Series*, vol. 210, p. 11, dec 2013.

[11] E. D. Team, "Using different moves," 2024. Accessed: 2024-08-15.

[12] V. Williams, "Location of the rotation axis of a tumbling cylindrical earth satellite by using visual observations part 1: Theory," *Planetary and Space Science*, vol. 27, pp. 885–890, 1979.